CORA Cork Open Research Archive
Cartlann Taighde Oscailte Chorcaí

Title	Ultralow-crosstalk, strictly non-blocking microring-based optical switch
Authors	Cheng, Qixiang;Dai, Liang Yuan;Abrams, Nathan C.;Hung, Yu-Han;Morrissey, Padraic E.;Glick, Madeleine;O'Brien, Peter A.;Bergman, Keren
Publication date	2019-01-16
Original Citation	Cheng, Q., Dai, L. Y., Abrams, N. C., Hung, Y.-H., Morrissey, P. E., Glick, M., O'Brien, P. and Bergman, K. (2019) 'Ultralow-crosstalk, strictly non-blocking microring-based optical switch', Photonics Research, 7(2), pp. 155-161. doi: 10.1364/PRJ.7.000155
Type of publication	Article (peer-reviewed)
Link to publisher's version	http://www.osapublishing.org/prj/abstract.cfm?URI=prj-7-2-155 - 10.1364/PRJ.7.000155
Rights	© 2019 Chinese Laser Press. Published by Optical Society of America. One print or electronic copy may be made for personal use only. Systematic reproduction and distribution, duplication of any material in this paper for a fee or for commercial purposes, or modifications of the content of this paper are prohibited.
Download date	2026-11-14 15:05:14
Item downloaded from	https://hdl.handle.net/10468/7501

UCC
University College Cork, Ireland
Coláiste na hOllscoile Corcaigh

To be published in Photonics Research:

Title: Ultralow-Crosstalk, Strictly Non-Blocking Microring-Based Optical Switch
Authors: Qixiang Cheng,Nathan Abrams,Yu-Han Hung,Padraic Morrissey,Madeleine Glick,Peter O
Accepted: 29 November 18
Posted 19 December 18
Doc. ID: 345596

Published by

OSA®

The Optical Society

Ultralow-Crosstalk, Strictly Non-Blocking Microring-Based Optical Switch

QIXIANG CHENG, [1,*] LIANG YUAN DAI, [1] NATHAN C. ABRAMS, [1] YU-HAN HUNG, [1] PADRAIC E. MORRISSEY, [2] MADELEINE GLICK, [1] PETER O'BRIEN, [2] AND KEREN BERGMAN [1]

[1] *Department of Electrical Engineering, Columbia University, New York, NY 10027, USA*
[2] *Tyndall National Institute, University College Cork, Cork, Ireland*
**Corresponding author: qc2228@columbia.edu*

Received XX Month XXXX; revised XX Month, XXXX; accepted XX Month XXXX; posted XX Month XXXX (Doc. ID XXXXX); published XX Month XXXX

We report on the first monolithically integrated microring-based optical switch in the switch-and-select architecture. The switch fabric delivers strictly non-blocking connectivity while completely canceling the first-order crosstalk. The 4×4 switching circuit consists of eight silicon microring-based spatial (de-)multiplexers interconnected by a Si/SiN dual-layer crossing-free central shuffle. Analysis of the on-state and off-state power transfer functions reveals the extinction ratios of individual ring resonators exceeding 25 dB, leading to switch crosstalk suppression of up to over 50 dB in the switch-and-select topology. Optical paths are assessed showing losses as low as 0.1 dB per off-resonance ring and 0.5 dB per on-resonance ring. Photonic switching is actuated with integrated micro-heaters to give ~24 GHz passband. The fully packaged device is flip-chip bonded onto a PCB breakout board with UV-curved fiber array. © 2018 Chinese Laser Press

http://dx.doi.org/10.1364/AO.99.099999

1. Introduction

Modern datacenters increasingly rely on the optical interconnect for delivering critical communication connectivity among numerous servers. The photonic switch is a potential key element to meet the growing interconnection performance requirements in datacenter architectures [1]. Several technologies can enable spatial or wavelength-selective optical switching, including micro-electro mechanical systems (MEMS) [2, 3], liquid crystals on silicon (LCOS) [4], beam-steering [5], semiconductor optical amplifiers (SOAs) [6, 7], Mach-Zehnder interferometers (MZIs) [8-11], micro-ring resonators (MRRs) [12, 13], and wavelength routing with tunable lasers [14]. Optical switching engines leveraging free-space optics have been commercialized, i.e. 3D MEMS, LCOS and beam-steering; however, the rigorous calibration and installation of discrete components introduce considerable complexity that is ultimately reflected in the cost per port. To ensure low cost per port and eventual data center adoption, optical switching technologies must demonstrate a path towards high volume manufacture. This is most likely to be implemented through lithography based fabrication and high-level integration [1].

Integrated photonic switch fabrics have been extensively explored in Indium Phosphide [7, 15] and silicon [3, 9-13, 16] platforms. Benefiting from the CMOS industry's developed fabrication and manufacturing infrastructures, silicon photonic devices have quickly matured to monolithic integration of tens of thousands of components [3, 9, 10]. The large index contrast between the core (silicon) and cladding (silica) layers enables strong confinement of the lightwave and thus leads to a much smaller device footprint. Silicon exhibits a strong thermo-optic (T-O) coefficient (1.8×10^{-4} K-1), which can be leveraged to tune the phase in tens of microseconds [17]. To benefit from nanosecond-scale switching times, the free-carrier dispersion effect offers the best all-silicon solution for electro-optic (E-O) switch fabrics.

The first demonstration of a μm-scale silicon ring resonator by Xu et al. stimulated the research of MRR-based photonic integrated circuits [18]. Because of their small footprint and low power consumption, silicon MRRs have been extensively studied as modulators, filters, and (de-)multiplexers. To date, MRR-based optical switches have been primarily implemented in crossbar-based topologies, such as the 8×7 optical crossbar switch [12] and the 4×4 two-stage cascaded crossbar switch [13]. The wavelength-selective nature of MRR unit requires wavelength alignment across the switching circuit, and various schemes for fast and efficient wavelength locking have been demonstrated [19-21]. The crossbar-type topology fits the add-drop nature of MRR unit, but the switch performance is limited by the large path-dependent loss and the first-order crosstalk.

In this paper, we present the design and thorough characterization of the first monolithic microring-based optical switch implemented in the switch-and-select topology. This design offers strictly non-blocking connectivity and fully blocks the first-order crosstalk. Si/SiN two-layered structure with escalating couplers is leveraged to eliminate

waveguide crossings in the central shuffle network. Preliminary test results can be found in [22]. Here, we present detailed analysis on the device performance from component-level to circuit-level showing a full power map across all electrically-connected paths, revealing ultralow-crosstalk impairment. The on-off extinction for individual ring resonators is examined. The passband of optical connections are measured and the bit error rate (BER) performance of 12.5 Gb/s data routing across the switch is verified. Discussion on the switch scalability is also provided. This demonstration shows a clear pathway towards high-performance optical switching circuits for data center applications.

2. Design, fabrication and packaging

A. Topology

The switch-and-select topology was first implemented using MZI switching elements [11]. It comprises two linear switching arrays connected by a passive central shuffle network, as shown in Fig. 1a. Each 1×N/N×1 switching unit is arranged in a cascading structure of $\log_2 N$ stages with MZI cells, resulting in a total number of switching stages being $2\log_2 N$. In this topology, each pair of input and output switching array is dedicated to a specific input to an output path, offering strictly non-blocking connectivity.

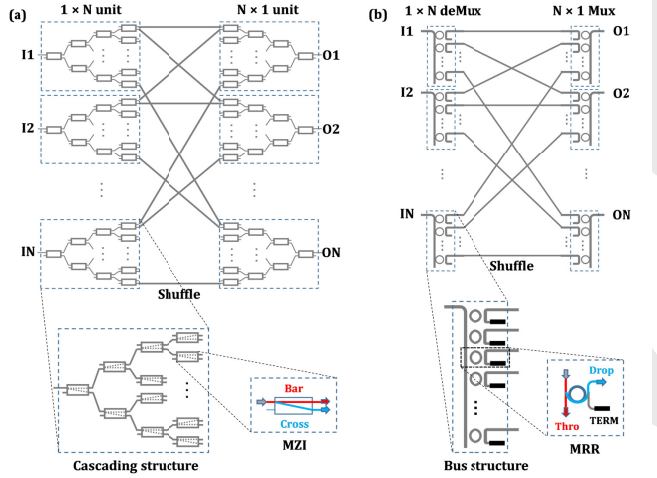


Fig. 1. (a) Switch-and-select topology with MZI elements arranged in a cascading structure. (b) Modified switch-and-select topology with MRR-based spatial (de)multiplexers.

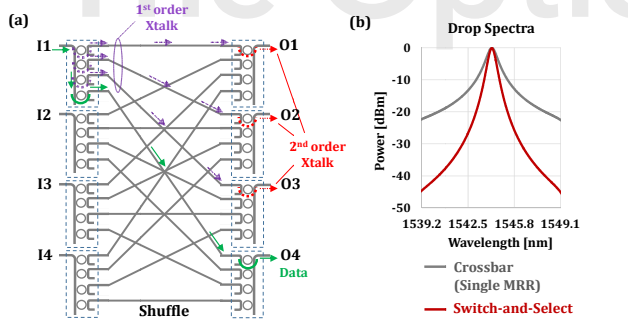


Fig. 2. (a) Schematic of a 4×4 switch-and-select switching circuit. Green, dashed purple and dotted red arrows outline paths for data, first-order crosstalk and second-order crosstalk, respectively. The solid semi-circles on MRRs indicate on-resonance coupling while dashed semi-circles represent off-resonance coupling. (b) Comparison of simulated drop spectrum of a single MRR element in a crossbar switching device and the switch-and-select structure.

The switch-and-select architecture, however, can be considerably simplified by using MRR add-drop filters assembled in a 1×N bus structure acting as spatial (de)multiplexers, as shown in Fig. 1b. Scale-up of such a design only requires adding microrings to the bus waveguides, which effectively reduces the scaling overhead in loss compared to that of the cascading scheme. The proposed design also maintains the number of drop (i.e. resonating) microrings in any path at two. An N×N switch-and-select switching circuit has in total $2N^2$ MRR elements. The central passive shuffle connects the i^{th} ring (element A) in the j^{th} 1×N input unit to the j^{th} ring (element B) in the i^{th} N×1 output unit. This brings a further advantage of self-routing as the optical connection of input i to output j occurs only when both element A and B rings are on resonance. The rest of the MRRs on the input and output units are adequately detuned from the resonance to ensure the maximum crosstalk suppression.

The MRR-based switch-and-select topology fully blocks the first-order crosstalk. For instance, in the 4×4 device illustrated in Fig. 2a, the optical path connects input 1 to output 4 (highlighted by green arrows) and the first order crosstalk leakage to the off-resonance rings (outlined by purple arrows at the 1st, 2nd and 3rd microring) will get suppressed by another detuned microring at the output stage (marked by red arrows) before adding to the signal, hence experiencing two degrees of attenuation. This lowers the switch crosstalk level to the square of a single MRR element. Figure 2b compares the simulated drop spectrum of a single MRR element, e.g. in a crossbar switching device, and the switch-and-select structure. The latter exhibits a much sharper spectral edge. In this design, the add-drop MRR element is better to operate close to its critical coupling to maximize the extinction of resonance and minimize the drop loss. Detailed design space exploration of silicon MRR element can be found in [23].

It has been recognized that the fundamental limitation to the scalability of the switch-and-select topology is the waveguide crossings in the central shuffle network [24], which interconnects $N^2 \times N^2$ waveguides from the two linear switching arrays. Therefore, in this work, we investigate the dual-layer shuffle network that eliminates waveguide crossings.

B. Device design and fabrication

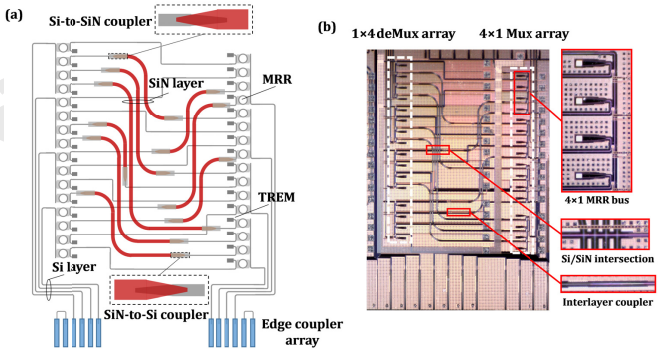


Fig. 3. (a) Schematic layout of the 4×4 MRR-based switch-and-select switching fabric with insets showing the interlayer couplers. (b) Microscope photo of the fabricated device with insets of the enlarged 4×1 MRR-based spatial multiplexer, the Si/SiN intersections and the interlayer coupler.

The layout of the 4×4 microring-based switch-and-select switching circuit is schematically shown in Fig. 3a. It comprises 32 add-drop ring resonators with integrated micro-heaters for on-chip tuning. Terminations are placed at the through port to eliminate optical

reflections. The central shuffle network is implemented in a Si/SiN dual-layer structure with interlayer couplers, enabling a SiN waveguide to pass over a Si waveguide at intersections. Key parameters for such a dual-layer device include the width of SiN waveguide (1 μm used in this work) and the separation between the two layers, determining the mode interaction and thus the loss and interlayer crosstalk. The intersections of Si and SiN waveguides should be maintained at 90 degrees for optimized performance. In this design a few compromises are made for the intersections due to the limited chip space. An edge coupler array is used to couple light in and out of the chip. Two pairs of looped-back couplers are introduced to facilitate the coupling process.

The device was taped out using standard PDK elements through the AIM Photonics MPW run. A microscope photo of the fabricated device is shown in Fig. 3b. The add-drop ring filters are placed at a pitch of 100 μm and the measured shift of resonance shows a thermal efficiency of 1 nm/mW [17]. The switch fabric has a compact footprint of 1.5×2.4 mm² with 32 control electrodes and 2 common grounds. The edge coupler array has a pitch of 127 μm.

C. Packaging

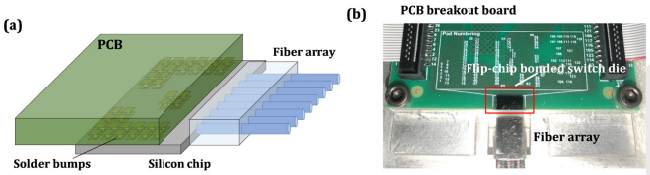


Fig. 4. (a) Schematic of silicon die flip-chip bonded onto a PCB breakout board using solder bumps. Fiber array is attached to the edge of silicon chip. (b) Photo of the packaged AIM chip.

The fabricated chip was packaged by the Tyndall National Institute using a flip-chip bonding process, as shown schematically in Fig. 4a. The bare chip, with bond pads of pitch 100um, were first gold studded and then solder was deposited using a PacTech solder jetter. The solder used in the process was SAC305, which has a 220 C melting point and provides solder balls with nominal diameters of 50 μm. The PIC was flip-chip bonded onto a custom designed PCB breakout board. The board and PIC were co-designed, so that after bonding the PIC overhangs the edge of the PCB by ~150 μm. This overhang allowed a lidless, 48 channel fiber array to be butt coupled to the PIC. The fiber array was optically aligned to the waveguides and attached using a UV curable epoxy. Ribbon cables were used to fan out the electrical connections. The packaged device was mounted onto an aluminum assembly and the completed package is shown in Fig. 4b.

3. Characterization

A. Optical power map

The operation of the optical switching circuit is first characterized in terms of on-state and off-state power transfer functions for each path. This gives a full optical power map of the device showing the optical insertion loss and crosstalk ratio across different paths. Figure 5a shows the test-bed. A tunable laser is used to launch a continuous-wave signal at the wavelength of 1542.3 nm, which is selected to be close to the half free spectral range (FSR) of MRRs to the resonance for maximum extinction. The control scheme is schematically shown by Fig. 5b. This also ensures that the operating wavelength has the minimum interaction with the bypass ring resonators. The on-state and off-state for each path are identified by tuning the bias voltage to reach the highest and lowest output power, respectively. The output is connected to an optical spectrum analyzer (OSA) to record both the peak transfer power and the spectrum. Figure 6 shows the measured optical power map of the 4×4 MRR-based switch-and-select device with the red rectangle outlining the crosstalk leakage. Data on 13 optical paths are recorded out of the total 16 paths due to 3 electrical open circuits. Measurement on the looped-back edge couplers indicates a coupling loss between the chip and fiber of 5.5 dB per facet.

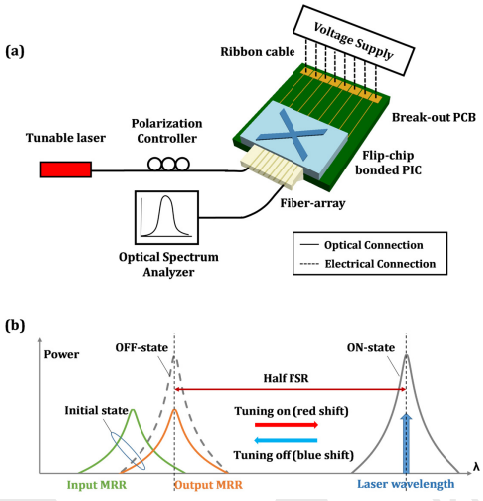


Fig. 5. (a) Schematic of the device test-bed. (b) Schematic of the control scheme of the switch-and-select switching circuit for on- and off-state.

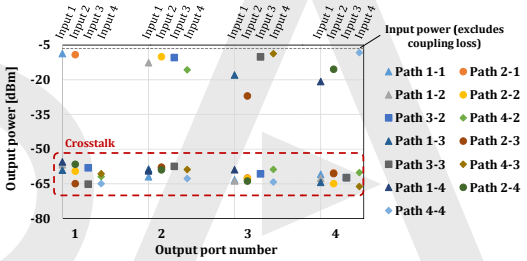


Fig. 6. Measured optical power map of the 4×4 MRR-based switch-and-select device. The red rectangle outlines the crosstalk leakage.

B. Optical loss analysis

Optical paths exhibit on-chip losses in the range of 1.8 to 20.4 dB as presented in Fig. 6. The large path-dependent loss is attributed to the high excess loss of escalating to and from the SiN layer. The passive loss of each path is a linear combination of different components; however, a large variation was observed for the SiN elements. As mentioned in section 2.B, the few intersections that have an angle of < 90 degrees between Si and SiN waveguides do indeed compromise the loss but it is suspected that the SiN waveguide and bending structure bring about excess loss, which requires further investigation.

Referring back to Fig. 3a, path 1-1 and 4-4 are both defined only in the Si layer and have no interaction with the SiN layer, representing the optimal cases. They both incorporate three off-resonance MRRs and two on-resonance ones; therefore, the 0.5 dB difference in loss (1.8 dB for path 4-4 and 2.3 dB for path 1-1) comes from the signal propagation in different waveguide lengths, showing the Si waveguide propagating loss to be 2.5 dB/cm.

The Si/SiN intersection loss and the interlayer coupling loss are assessed by two additional test structures, shown by Fig. 7a and 7b, respectively. The intersection loss is measured to be ~0.15 dB on the Si waveguide. This is believed to be primarily caused by the mode interaction with the overpassed SiN layer due to the limited separation

distance. Study of the Si/SiN interlayer mode-interaction for transmission loss and crosstalk as a function of the separation using Lumerical FDTD software is shown in Fig. 7c. Minimizing the dual layer performance penalty requires > 450 nm separation. Future designs will leverage the triple layer platform developed by AIM photonics, in which a SiN transfer layer is inserted in between to ensure adequate separation between the Si and the second SiN layer. The interlayer couplers are characterized to have 4 dB loss per pair (2 dB per facet), which is quite off from the predicted results. This could well be caused by imperfect fabrication and can be improved in the future. Fitting the test results back to paths 1-2, 2-1, 4-3 and 4-4 that have various numbers of off-resonance rings, we can estimate the loss for the MRR drop and through states, which are 0.5 dB and 0.1 dB, respectively. The component-level loss estimation is summarized in Table 1.

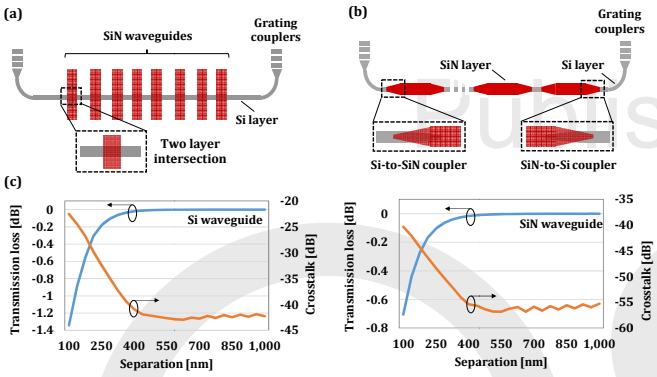


Fig. 7. Schematic of test structures for (a) the Si/SiN two layered intersections, and (b) Si/SiN interlayer couplers. (c) Simulated insertion loss and crosstalk as a function of interlayer separation for the two-layer intersections using Lumerical FDTD software. The left and right chart show the results for Si and SiN waveguide, separately.

Table 1. Component-level loss estimation

Item	Loss
Si waveguide propagation	2.5 dB/cm
MRR drop	0.5 dB
MRR through	0.1 dB
Si/SiN intersection	0.15 dB
Si/SiN interlayer coupler	2 dB/facet
Edge coupler	5.5 dB/facet

C. Extinction and crosstalk

Off-state signals are required to be maximally extinguished. The sum of leakage from any off-state paths contributes to a path dependent crosstalk. The on-off extinction of the individual ring resonators is thus a key parameter.

Figure 8 presents the crosstalk breakdown measurements to reveal the on-off extinction of individual ring elements that contribute to the crosstalk suppression. As illustrated by Fig. 8a, data is routed through path 2-2 and the crosstalk leakage is monitored at output 1. In the outlined input 1×4 spatial deMux unit, the first MRR (element *a*) is at off-resonance state to let the data bypass while the second ring element (element *b*) is on resonance to drop the signal. The data is then routed to output 2 by tuning the corresponded MRR at the second output 4×1 Mux unit. The measured spectrum is shown by Fig. 8b. The second MRR at the first output 4×1 Mux unit (element *c*) that receives the crosstalk leakage is first set at on-resonance. The spectrum is presented by the light blue line in Fig. 8c and comparing to that of the Fig. 8b, the difference shows the first-order crosstalk suppression between *a* ring and *b* ring (25.1 dB). The subsequent tuning of *c* ring to off-resonance (shown by the dark blue line in Fig. 8c) maximally extinguishes the off-state leakage to output 1. The contrast between the light blue and dark blue lines discloses the on-off extinction of *c* ring (25.6 dB) while comparing the light blue line to the grey line in Fig. 8b shows the full crosstalk suppression between output 1 and 2 (50.7 dB).

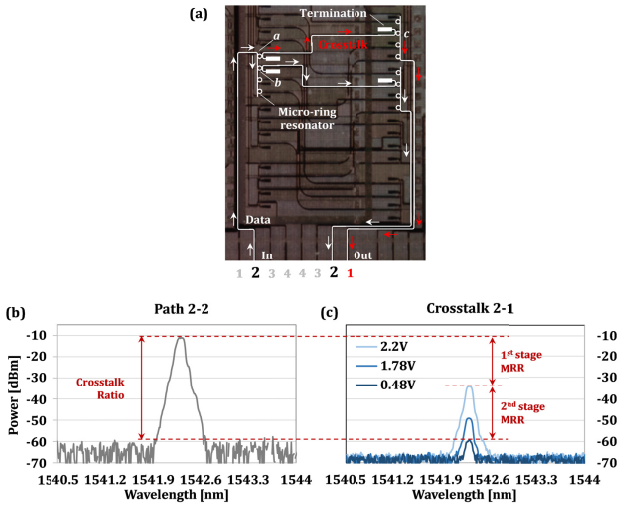


Fig. 8. Crosstalk breakdown measurement. (a) Outlined optical paths under test: data routed in path 2-2 and the crosstalk leakage to output 1 (crosstalk 2-1). Measured power spectrum for (b) the data at output 2 and (c) crosstalk leakage at output 1 with thermal tuning on the 2nd stage output MRR to minimize the crosstalk leakage.

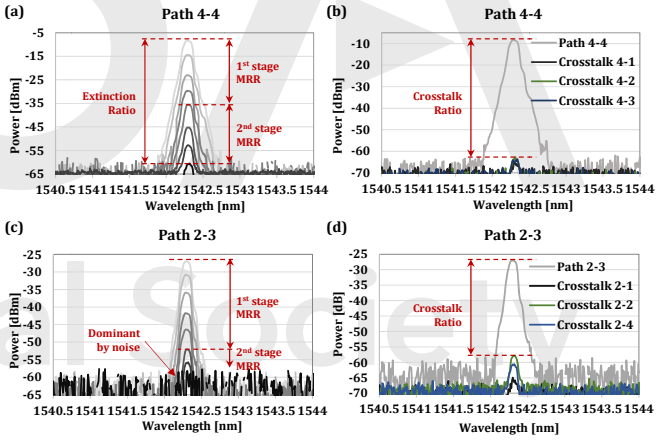


Fig. 9. (a) Power tuning for path 4-4 showing the path extinction ratio and the breakdown in on-off extinction from the 1st and 2nd stage MRRs. (b) Crosstalk leakage to output 1, 2 and 3 for path 4-4. (c) Power tuning for path 2-3 and (d) crosstalk leakage for path 2-3.

We further examine the breakdown in on-off extinction of individual ring resonators for path extinction ratios. All measured ring resonators feature an on-off extinction of larger than 25 dB. Figure 9 shows detailed measurement on two representative paths of 4-4 and 2-3, showing the best and worst cases. Path 4-4 exhibits an extinction ratio of 52.7 dB with the contribution of 27.3 dB and 25.4 dB from the first and second stage MRR, respectively, as shown by Fig. 9a. The measured crosstalk ratio to output 1, 2 and 3 is presented in Fig. 9b (lower than -54.4 dB). For path 2-3, the first and second stage MRR

shows an on-off extinction of 25.6 dB and 26.1 dB, respectively; however, the OSA only sees the path extinction ratio of 31.4 dB which is limited by the noise floor (illustrated by Fig. 9c). The high path insertion loss also compromises the crosstalk ratio (below -31.6 dB), as shown in Fig. 9d. This, however, can be significantly improved by optimizing the component design and fabrication in the future.

D. Optical passband and BER measurement

An Erbium-doped fiber amplifier (EDFA)-based broadband source is used at the input to verify the passband of optical connections. The spectra are recorded using the OSA with a resolution of 0.1 nm. The normalized spectra of a set of representative paths for 1-1, 1-4, 2-1, 2-3, 3-3 and 4-4 are shown in Fig. 7, indicating a passband of ~24 GHz.

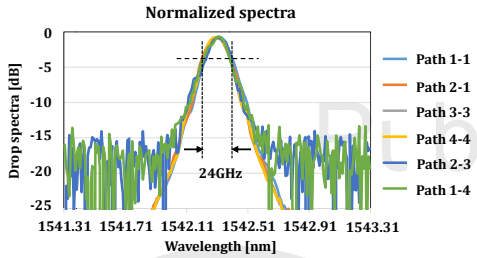


Fig. 10. Normalized spectra of a set of representative paths. Resolution is set at 0.1 nm.

Measurements of the BER performance of the switch were performed. A 12.5 Gb/s amplitude-shift keying coded pseudorandom binary sequence (PRBS) with a length of 2^{31} -1 is employed to modulate the tunable laser through an external Mach-Zehnder modulator. The modulated data then enter the switch. The output from the device is fed into an EDFA which is filtered with a band pass filter before connecting to the error detector. The BER as a function of optical received power is recorded. Negative power penalties as the difference in received optical power required achieving a BER of 10^{-9} with the presence and absence of the switch are recorded for all measured paths, in the range of -1.7 to -1.0 dB. It should be noted that an optical attenuator is used to emulate the switch insertion loss for back-to-back (B2B) BER measurement. Detailed test results for the two representative paths, i.e. 4-4 and 2-3, are presented in Fig. 11a and 11b, showing a power penalty of -1.7 dB and -1.3 dB, respectively. It can be seen that the slope of the fitted lines for both measured BER data remain nearly unchanged. This means that the device induced inter-symbol-interference (ISI) is negligible as the passband is wider than the bandwidth of the modulated signal.

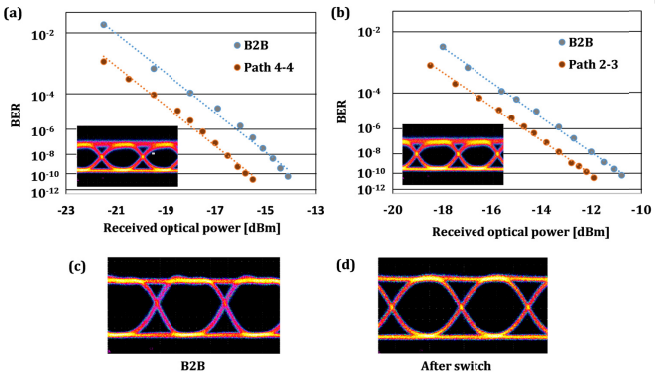


Fig. 11. BER as a function of received optical power at 12.5 Gb/s for (a) path 4-4 and B2B, and for (b) path 2-3 and B2B. Insets show eye diagrams after switch. (c) and (d) show the amplified eye diagrams for B2B and path 4-4 @ 0dBm.

The negative power penalty could well be attributed to the filtering nature of microrings that compensate the signal distortion due to the nonlinearity of the lightwave modulator [25]. For a closer examination, the amplified B2B eye diagram is shown in Fig. 11c exhibiting weak, yet visible overshoots and uneven eye crossings. The uneven eye crossings that come from the nonlinearity of the lightwave modulator in turn decrease the detection sensitivity [26]. A clearer eye diagram with even eye crossings is recorded after the switch, as presented in Fig. 11d.

E. Switching power and reconfiguration time

The on-state bias for the microring resonators lies in the range of 2.1 to 2.7 V while the off-state bias ranges from 0 to 0.65 V. The consumed tuning power to half FSR is at 8 to 10 mW and the total power consumption per path (including both on-state and off-state tuning) is roughly at 20 mW. At a full switch load, the 4×4 optical switching circuit is estimated to draw 80 mW power.

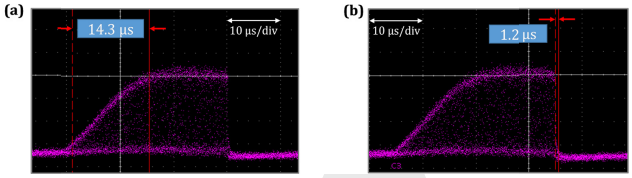


Fig. 11. Measured optical time-domain response of the thermo-optic switch. The cursors show the 10% to 90% power points for (a) the rise edge and (b) the fall edge.

The optical reconfiguration times were characterized by measuring the optical time-domain response of the thermo-optic switch. A 15 KHz electrical square-wave signal with a 50% duty cycle is applied to path 4-4. The time trace of the output signal that carries a 12.5 Gb/s NRZ data is recorded in Fig. 11. The rise and fall time of the switch is measured to be 14.3 µs and 1.2 µs (10% to 90%), respectively.

4. Discussion and conclusion

This paper presents the first microring-based optical switching circuit in switch-and-select topology. The demonstrated 4×4-port device consists of 32 thermally-actuated ring resonator-based switch elements with losses of 0.5 dB per on-resonance ring and 0.1 dB per off-resonance ring. Over 25 dB on-off extinction of individual ring resonators is achieved. The primary figure of merits for the scalability and performance in silicon-based optical switches are loss and crosstalk [27]. Scale-up of the switch-and-select devices only requires adding bypass rings in the linear switch arrays at 0.1 dB loss penalty per ring. Designs for Si/SiN interlayer coupling loss below 0.1 dB are already available [28] and the SiN waveguide propagation loss can be as low as 0.1 dB/m [29], offering a strong potential for ultra-low loss shuffle networks in large port count switches. By lowering the crosstalk ratio to the square of a single MRR element, an ultra-high crosstalk immunity of up to over 50 dB can be obtained. This device shows great potential for high-performance switching applications in datacenters.

Funding Information. Air Force Research Laboratory (FA8650-15-2-5220); ARPA-E ENLITENED project (DE-AR00000843); Rockport Networks Inc.; European Packaging Pilot Line 'PIXAPP' (H2020-731954).

References

1. Q. Cheng, S. Rumley, M. Bahadori and K. Bergman, *Photonic switching in high performance datacenters [Invited].* Optics Express, 2018. **26**(12): p. 16022-16043.
2. J. Kim, C. J. Nuzman, B. Kumar, D. F. Lieuwen, J. S. Kraus, A. Weiss, C. P. Lichtenwalner, A. R. Papazian, R. E. Frahm, N. R. Basavanhally, D. A. Ramsey, V. A. Aksyuk, F. Pardo, M. E. Simon, V. Lifton, H. B. Chan, M. Haueis, A. Gasparyan, H. R. Shea, S. Arney, C. A. Bolle, P. R. Kolodner, R. Ryf, D. T. Neilson, and J. V. Gates, *1100 x 1100 port MEMS-based optical crossconnect with 4-dB maximum loss.* IEEE Photonics Technology Letters, 2003. **15**(11): p. 1537-1539.
3. K. Kwon, T. J. Seok, J. Henriksson, J. Luo, L. Ochikubo, J. Jacobs, R. S. Muller and M. C. Wu. *128×128 Silicon Photonic MEMS Switch with Scalable Row/Column Addressing*. in *Conference on Lasers and Electro-Optics*. 2018. San Jose, California: Optical Society of America.
4. B. Robertson, H. Yang, M. M. Redmond, N. Collings, J. R. Moore, J. Liu, A. M. Jeziorska-Chapman, M. Pivnenko, S. Lee, A. Wonfor, I. H. White, W. A. Crossland and D. P. Chu, *Demonstration of Multi-Casting in a 1 × 9 LCOS Wavelength Selective Switch.* Journal of Lightwave Technology, 2014. **32**(3): p. 402-410.
5. H. C. H. Mulvad, A. Parker, B. King, D. Smith, M. Kovacs, S. Jain, J. Hayes, M. Petrovich, D. J. Richardson and N. Parsons. *Beam-steering all-optical switch for multi-core fibers*. in *Optical Fiber Communication Conference*. 2017. Optical Society of America.
6. Q. Cheng, A. Wonfer, J. L. Wei, R. V. Penty, and I. H. White, *Low-energy, high-performance lossless 8×8 SOA switch*, in *Optical Fiber Communication Conference*. 2015, OSA Technical Digest (online) (Optical Society of America, 2015), paper Th4E.6.
7. R. Stabile, A. Albores-Mejia, and K. A. Williams, *Monolithic active-passive 16 × 16 optoelectronic switch.* Optics Letters, 2012. **37**(22): p. 4666-4668.
8. Q. Cheng, A. Wonfor, J. L. Wei, R. V. Penty and I. H. White, *Monolithic MZI-SOA hybrid switch for low-power and low-penalty operation.* Opt Lett, 2014. **39**(6): p. 1449-52.
9. K. Suzuki, R. Konoike, J. Hasegawa, S. Suda, H. Matsuura, K. Ikeda, S. Namiki and H. Kawashima. *Low Insertion Loss and Power Efficient 32 × 32 Silicon Photonics Switch with Extremely-High-Δ PLC Connector*. in *Optical Fiber Communication Conference Postdeadline Papers*. 2018. San Diego, California: Optical Society of America.
10. T. Chu, L. Qiao, W. Tang, D. Guo and W. Wu. *Fast, High-radix Silicon Photonic Switches*. in *2018 Optical Fiber Communications Conference and Exposition (OFC)*. 2018.
11. L. Chen and Y.-K. Chen, *Compact, low-loss and low-power 8×8 broadband silicon optical switch.* Optics Express, 2012. **20**(17): p. 18977-18985.
12. P. Dasmahapatra, R. Stabile, A. Rohit and K. A. Williams, *Optical Crosspoint Matrix Using Broadband Resonant Switches.* IEEE Journal of Selected Topics in Quantum Electronics, 2014. **20**(4): p. 1-10.
13. N. Sherwood-Droz, H. Wang, L. Chen, B. G. Lee, A. Biberman, K. Bergman and M. Lipson, *Optical 4×4 hitless silicon router for optical Networks-on-Chip (NoC).* Optics Express, 2008. **16**(20): p. 15915-15922.
14. Z. Pan, S. Fu, L. Lu, D. Li, W. Chang, D. Liu and M. Zhang, *On-chip cyclic-AWG-based 12 × 12 silicon wavelength routing switches with minimized port-to-port insertion loss fluctuation.* Photonics Research, 2018. **6**(5): p. 380.
15. Q. Cheng, M. Ding, A. Wonfor, J. Wei, R. V. Penty and I. H. White, *The Feasibility of Building a 64x64 Port Count SOA-Based Optical Switch*, in *2015 International Conference on Photonics in Switching (PS)*. 2015: Florence. p. 199-201.
16. A. Novack, Y. Liu, R. Ding, M. Gould, T. Baehr-Jones, Q. Li, Y. Yang, Y. Ma, Y. Zhang, K. Padmaraju, K. Bergmen, A. E. Lim, G. Lo and M. Hochberg. *A 30 GHz silicon photonic platform*. in *10th International Conference on Group IV Photonics*. 2013.
17. M. Bahadori, A. Gazman, N. Janosik, S. Rumley, Z. Zhu, R. Polster, Q. Cheng and K. Bergman, *Thermal Rectification of Integrated Microheaters for Microring Resonators in Silicon Photonics Platform.* Journal of Lightwave Technology, 2017: p. 1-1.
18. Q. Xu, B. Schmidt, S. Pradhan and M. Lipson, *Micrometre-scale silicon electro-optic modulator.* Nature, 2005. **435**: p. 325.
19. A. S. P. Khope, T. Hirokawa, A. M. Netherton, M. Saeidi, Y. Xia, N. Volet, C. Schow, R. Helkey, L. Theogarajan, A. A. M. Saleh, J. E. Bowers and R. C. Alferness, *On-chip wavelength locking for photonic switches.* Opt Lett, 2017. **42**(23): p. 4934-4937.
20. K. Padmaraju, D. F. Logan, T. Shiraishi, J. J. Ackert, A. P. Knights and K. Bergman, *Wavelength Locking and Thermally Stabilizing Microring Resonators Using Dithering Signals.* Journal of Lightwave Technology, 2014. **32**(3): p. 505-512.
21. C. Sun, M. Wade, M. Georgas, S. Lin, L. Alloatti, B. Moss, R. Kumar, A. H. Atabaki, F. Pavanello, J. M. Shainline, J. S. Orcutt, R. J. Ram, M. Popović and V. Stojanović, *A 45 nm CMOS-SOI Monolithic Photonics Platform With Bit-Statistics-Based Resonant Microring Thermal Tuning.* IEEE Journal of Solid-State Circuits, 2016. **51**(4): p. 893-907.
22. Q. Cheng, L. Y. Dai, M. Bahadori, N. C. Abrams, P. E. Morrissey, M. Glick, P. O'brien and K. Bergman, *Si/SiN Microring-Based Optical Router in Switch-and-Select Topology*, in *European Conference on Optical Communication (ECOC)*. 2018. paper We1C.3.
23. M. Bahadori, M. Nikdast, S. Rumley, L. Y. Dai, N. Janosik, T. Van Vaerenbergh, A. Gazman, Q. Cheng, R. Polster and K. Bergman, *Design Space Exploration of Microring Resonators in Silicon PhotonicInterconnects: Impact of the Ring Curvature.* Journal of Lightwave Technology, 2018. **36**(13): p. 2767-2782.
24. Q. Cheng, M. Bahadori, S. Rumley and K. Bergman. *Highly-scalable, low-crosstalk architecture for ring-based optical space switch fabrics*. in *2017 IEEE Optical Interconnects Conference (OI)*. 2017.
25. L. S. Yan, Y. Wang, B. Zhang, C. Yu, J. Mcgeehan, L. Paraschis and A. E. Willner, *Reach extension in 10-Gb/s directly modulated transmission systems using asymmetric and narrowband optical filtering.* Optics Express, 2005. **13**(13): p. 5106-5115.
26. J. Ruzbarsky, J. Turan and L. Ovsenik. *Effects act on transmitted signal in a fully optical fiber WDM systems*. in *2015 IEEE 13th International Scientific Conference on Informatics*. 2015.
27. Q. Cheng, M. Bahadori, M. Glick, S. Rumley and K. Bergman, *Recent advances in optical technologies for data centers: a review.* Optica, 2018. **5**(11): p. 1354-1370.
28. W. D. Sacher, Y. Huang, G. Lo and J. K. S. Poon, *Multilayer Silicon Nitride-on-Silicon Integrated Photonic Platforms and Devices.* Journal of Lightwave Technology, 2015. **33**(4): p. 901-910.
29. J. F. Bauters, M. J. R. Heck, D. D. John, J. S. Barton, C. M. Bruinink, A. Leinse, R. G. Heideman, D. J. Blumenthal and J. E. Bowers, *Planar waveguides with less than 0.1 dB/m propagation loss fabricated with wafer bonding.* Optics Express, 2011. **19**(24): p. 24090-24101.

Published by Optical Society